Journal of Geophysical Research: Solid Earth

Supporting Information for

Transient Aseismic Slip Following 2017 Mw 7.3 Sarpol-e Zahab, Iran, Earthquake: Possible Evidence for Fault Frictional Heterogeneity and Thin-skinned Shortening Following a Thick-skinned Basement-involved Faulting in the Zagros Fold-thrust Belt

Zelong Guo[1,2], Mahdi Motagh[1,2], Jyr-Ching Hu[3], Guangyu Xu[4], Mahmud Haghshenas Haghighi[2], Abbas Bahroudi[5] and Aram Fathian[6]

[1]GFZ German Research Centre for Geosciences, Department of Geodesy, Section of Remote Sensing,14473 Potsdam, Germany

[2]Institute for Photogrammetry and GeoInformation, Leibniz University Hannover, 30167 Hannover, Germany

[3]Department of Geosciences, National Taiwan University, 10617 Taipei, Taiwan

[4]Faculty of Geomatics, East China University of Technology, 330013 Nanchang, Jiangxi, China

[5]Exploration Department, School of Mining Engineering, Engineering Faculty, University of Tehran, 515-14395 Tehran, Iran

[6]Neotectonics and Natural Hazards Institute, RWTH Aachen University, 52064 Aachen, Germany

Contents of this file

Introduction

This supplementary material includes the information about the uniform coseismic slip model from nonlinear inversion (Text S1), thirteen supporting figures (From Figure S1 to S13) and three tables (Table S1 to S3) about the InSAR data and fault model constraints.

Text S1: Uniform coseismic slip model from nonlinear inversion

The multipeak particle swarm optimization (MPSO) approach, which is based on a hybrid minimization algorithm (e.g., Feng et al., 2013, 2014, 2017), was used for nonlinear global searching. The causative fault of the 2017 Sarpol-e Zahab earthquake is modeled as a single rectangular dislocation with uniform slip in a homogeneous, elastic half-space assuming a shear modulus of 33 GPa and a Poisson ratio of 0.25. We imposed constraints for the fault parameters (Table S3) by referring the published results. The preferred fault model is a blind, almost north-south trending (a strike of 354.7°), east-dipping (a dip of 17.17°) fault with a rake of 143.74°. The mainshock mainly ruptured a 40 km long and 18 km wide fault with a uniform slip about 3.7 m, the centroid depth from our nonlinear inversion is about 16 km (Figure S6), indicates the mainshock ruptured a basement-involved fault. The uncertainties of these model parameters are evaluated by a Monte Carlo bootstrap simulation technique with 100 simulations perturbed with observations noises based on VCM (Figure S6). Our preferred fault geometry is consistent with the uniform models proposed by previous studies (e.g., Feng et al., 2018; Barnhart et al., 2018; Wang and Bürgmann, 2020).

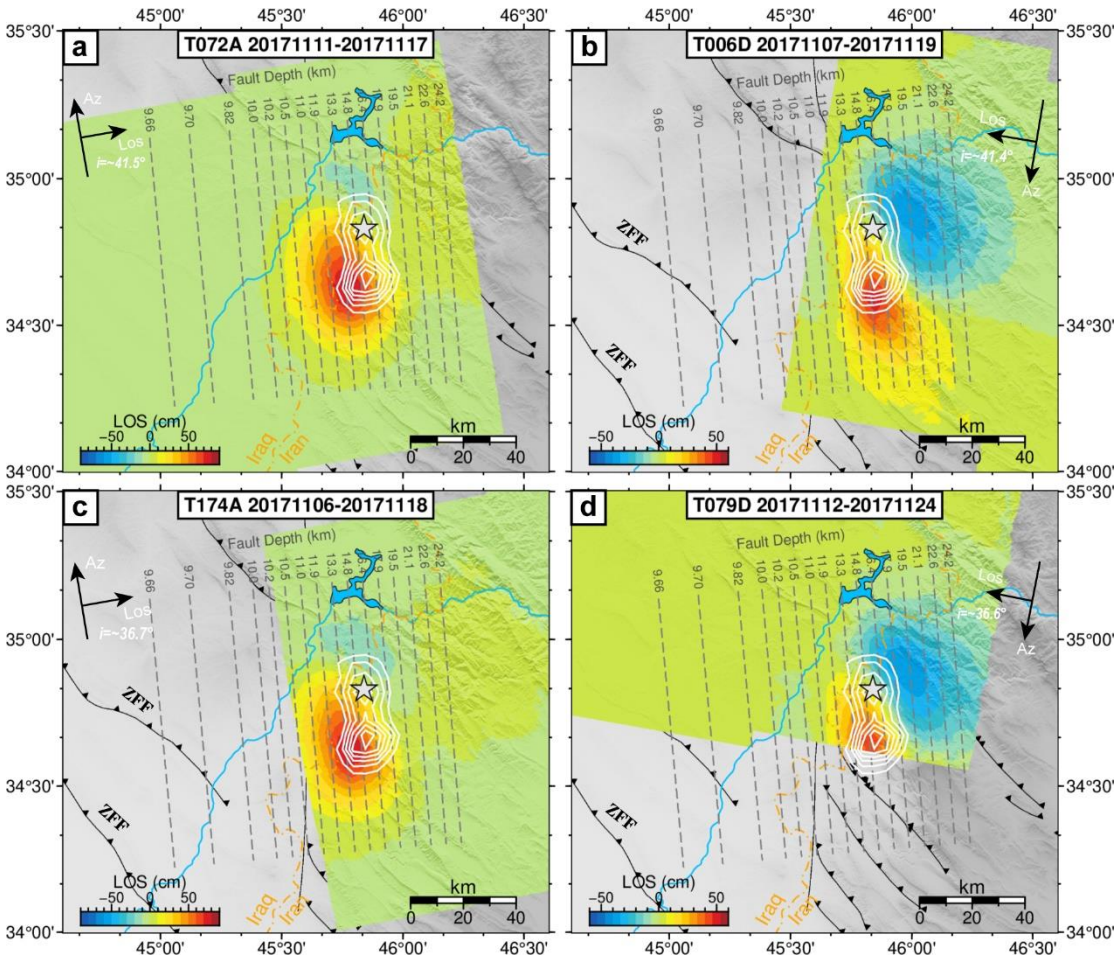

Figure S1. Coseismic interferograms from (a) T072A, (b) T006D, (c) T174A and (d) T079D of the 2017 Sarpol-e Zahab earthquake. Gray dashed lines represent the fault depth of the anti-listric model. White contours and gray star represent our preferred coseismic slip model at 1-m intervals and the epicenter of the Mw 7.3 mainshock, respectively.

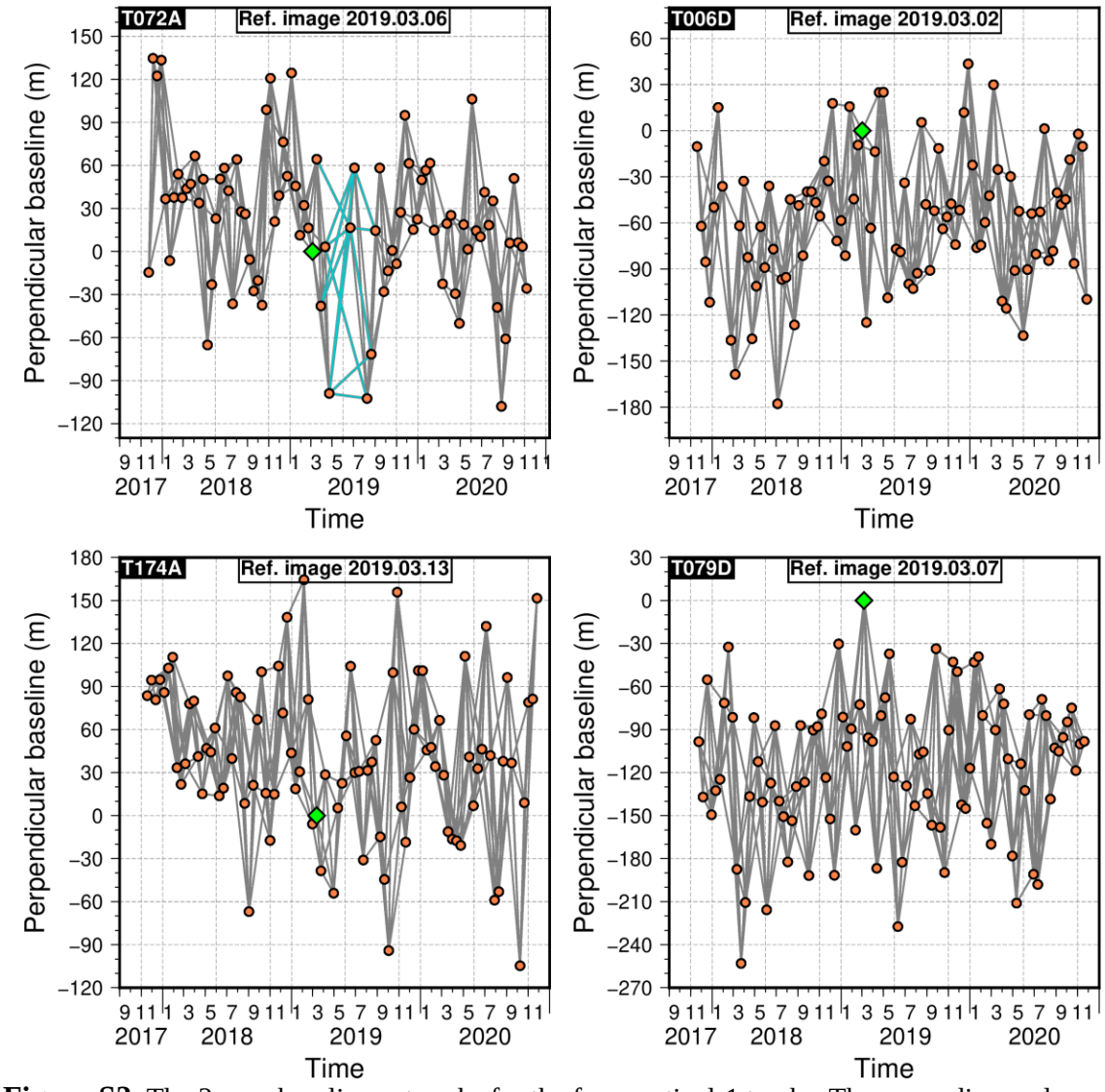

Figure S2. The 3-year baseline networks for the four sentinel-1 tracks. The green diamond represents the reference image. For T072A, there are only 83 single look complex (SLC) data from 23 November 2017 to 26 October 2020. Because there is a 60 days gap between April and June of 2019, thus we just re-selected 13 interferogram pairs (green lines) with 9 SLC data between 18 March 2019 and 02 September 2019, in order to form at least 3 interferogram pairs for every single SLC data.

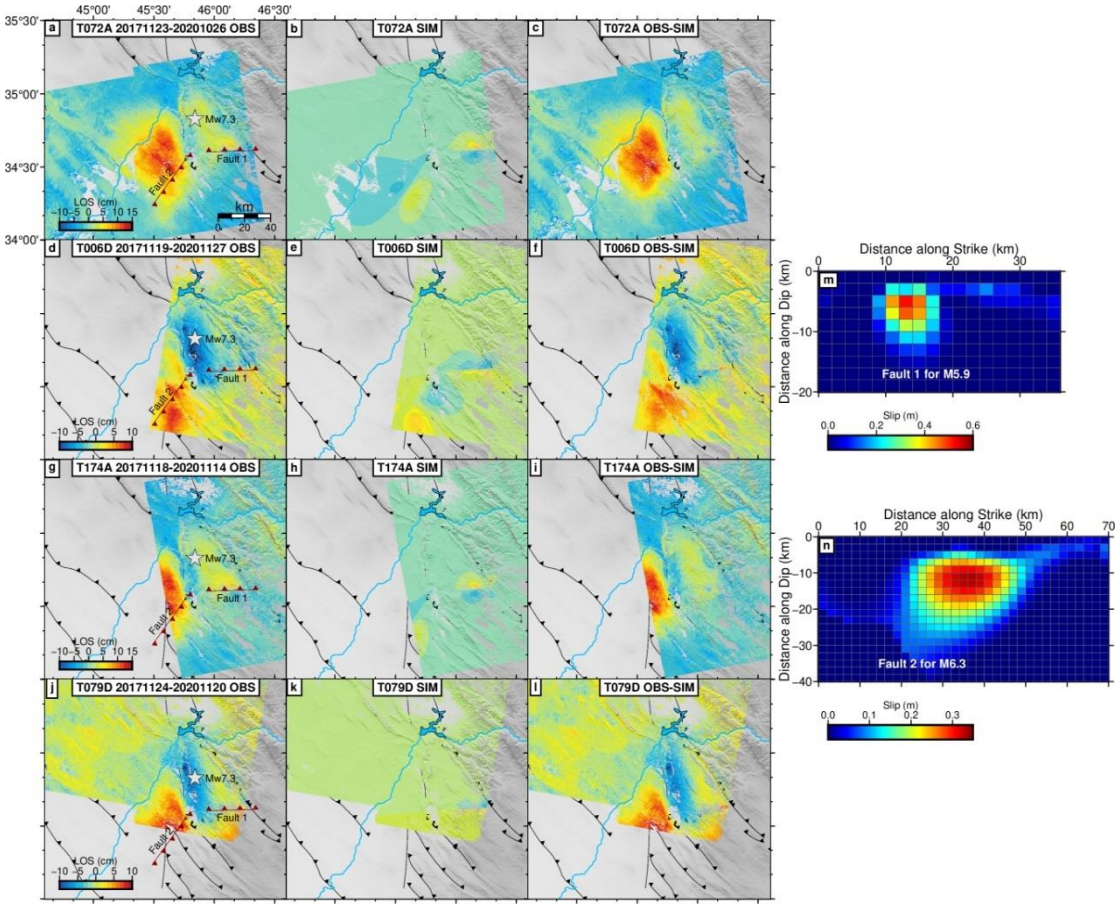

Figure S3. (a, d, g, j) are the 3-year postseismic deformation of 2017 Sarpol-e Zahab earthquake for T072A, T006D, T174A and T079D, respectively; (b, e, h, k) are the simulated surface displacements of the Mw 5.9 and Mw 6.3 earthquake for T072A, T006D, T174A and T079D, which are from the forwarding modeling with the fault models (m-n) proposed by Fathian et al. (2021); (c, f, i, l) are the cleaner results after the reducing of the simulations (b, e, h, k) from original observations (a, d, g, j). The gray star is the epicenter of the mainshock. The red faults (Fault 1 and Fault 2) are surface trace of fault models from Fathian et al. (2021).

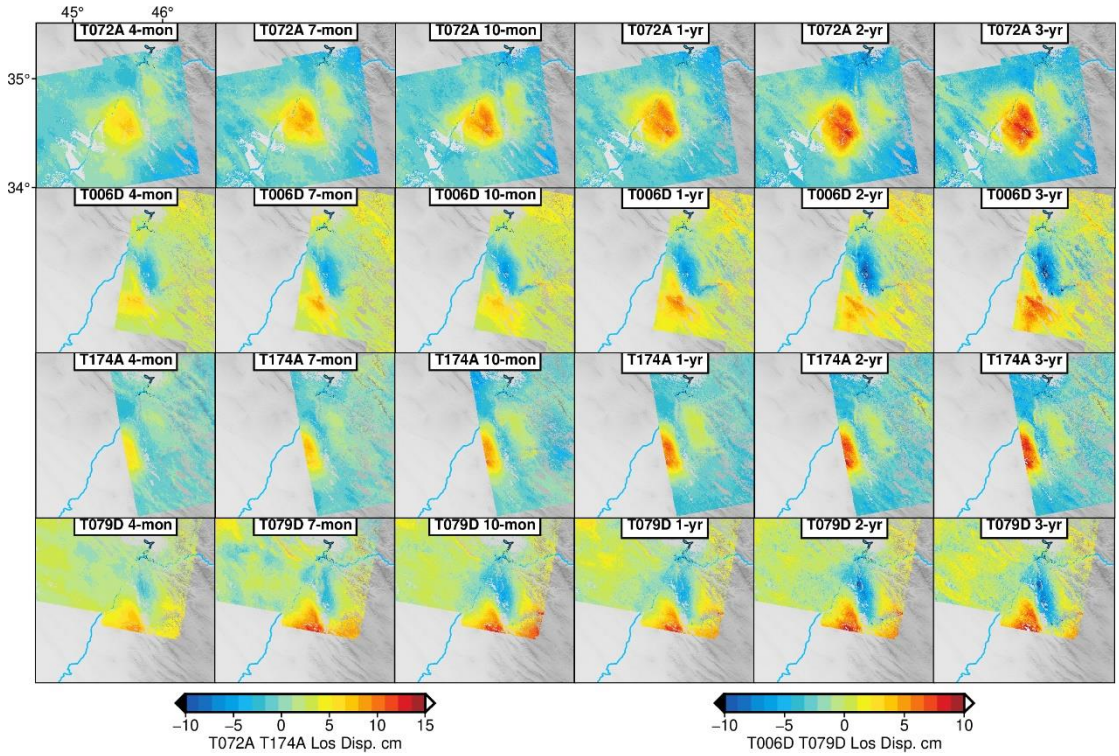

Figure S4. The InSAR time series of T072A, T006D, T174A and T079D after reducing the coseismic deformation of the 25 August 2018 Mw 5.9 and 25 November 2018 Mw 6.3 earthquake.

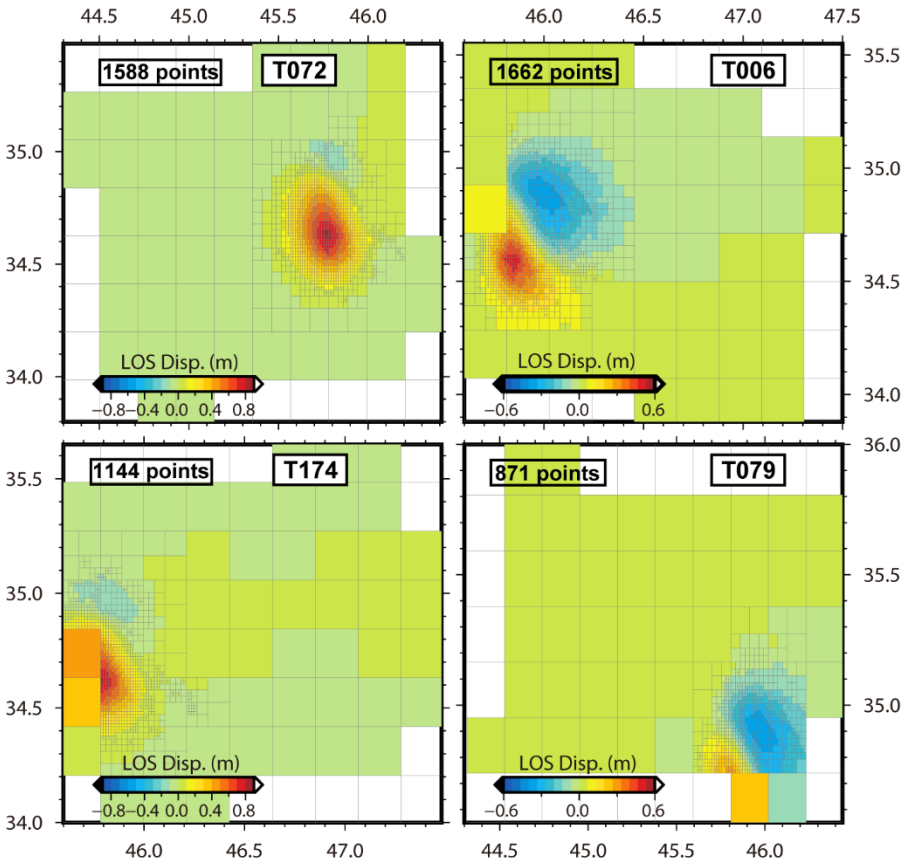

Figure S5. The downsampled points from 4-track coseismic interferograms with quadtree sampling approach (Jónsson et al., 2002), totally 5265 points.

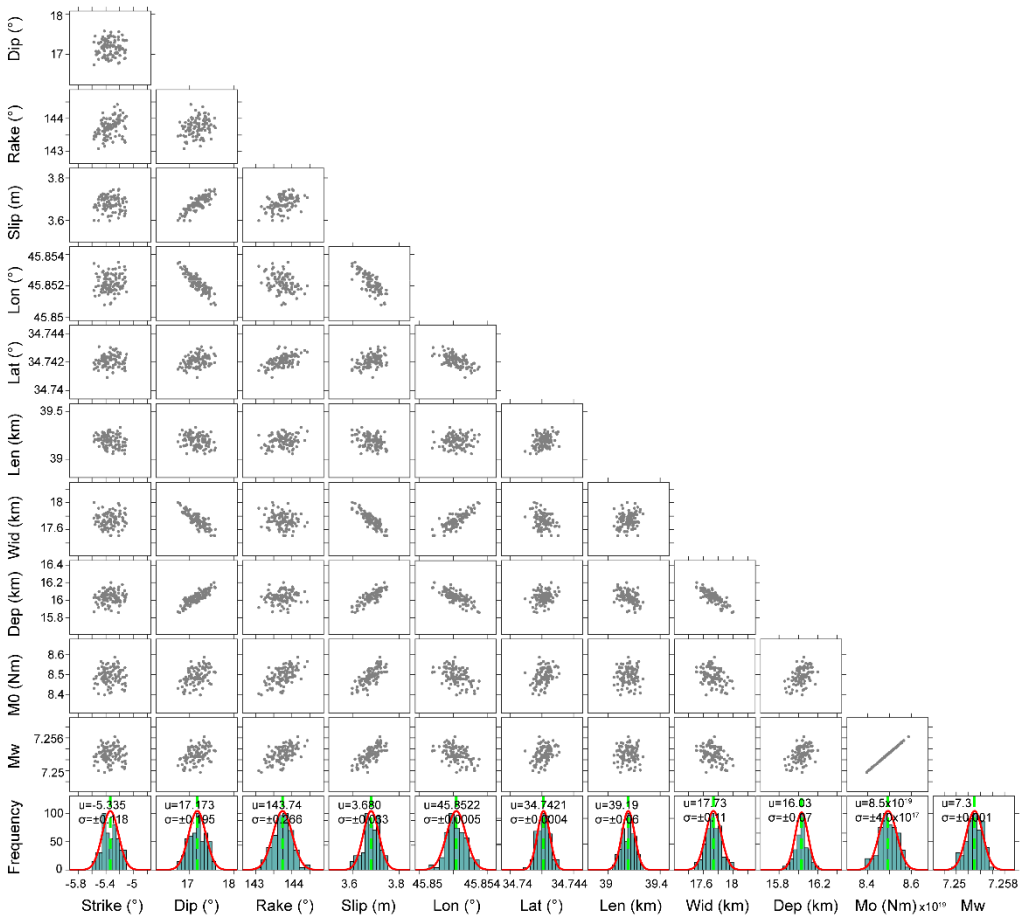

Figure S6. Nonlinear inversion results. The mean values (μ) and standard deviation (σ) of the fault parameters calculated by Monte Carlo method. The fault location and depth are centroid.

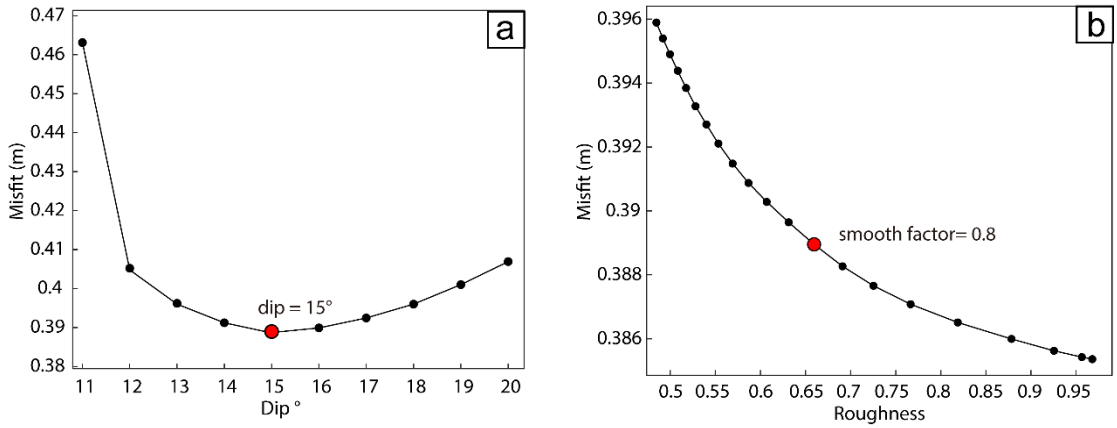

Figure S7. (a) Misfit for testing different dip angle of planar faults, the optimal dip angle is denoted by a solid red circle. (b) Trade-off curve between weighted misfit and the roughness of planar models, the optimal smooth factor is denoted by a solid red circle.

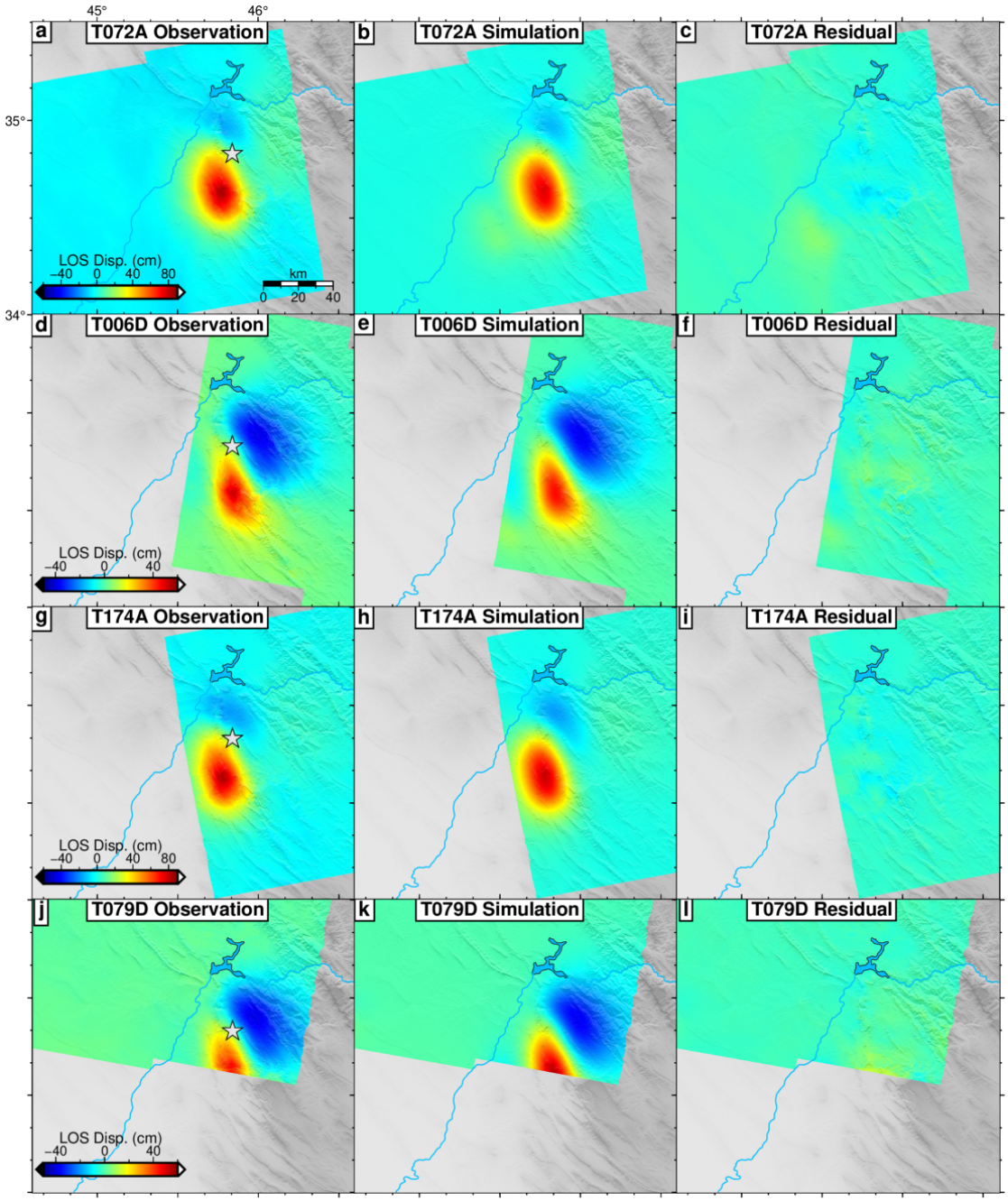

Figure S8. The observations, simulations and residuals of T072A (a-c), T006D (d-f), T174A (g-i) and T079D (j-l) based on the coseismic model. The gray star is the epicenter of the mainshock.

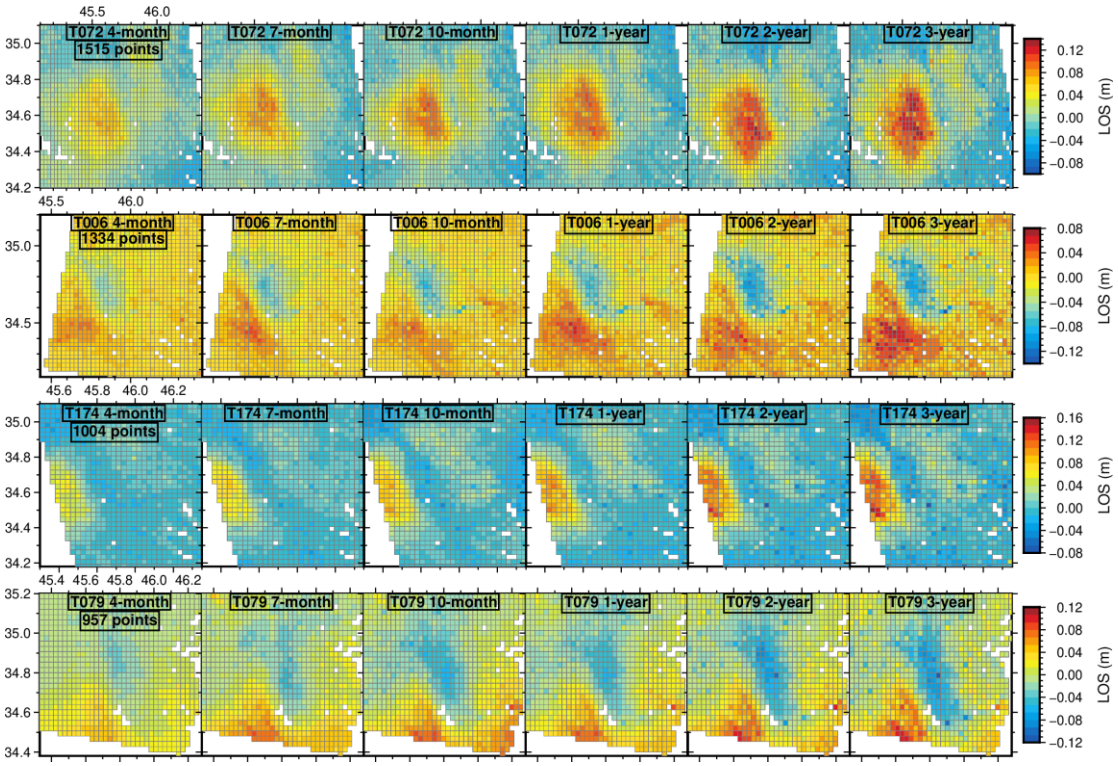

Figure S9. The downsampled points from 4-track postseismic InSAR time series.

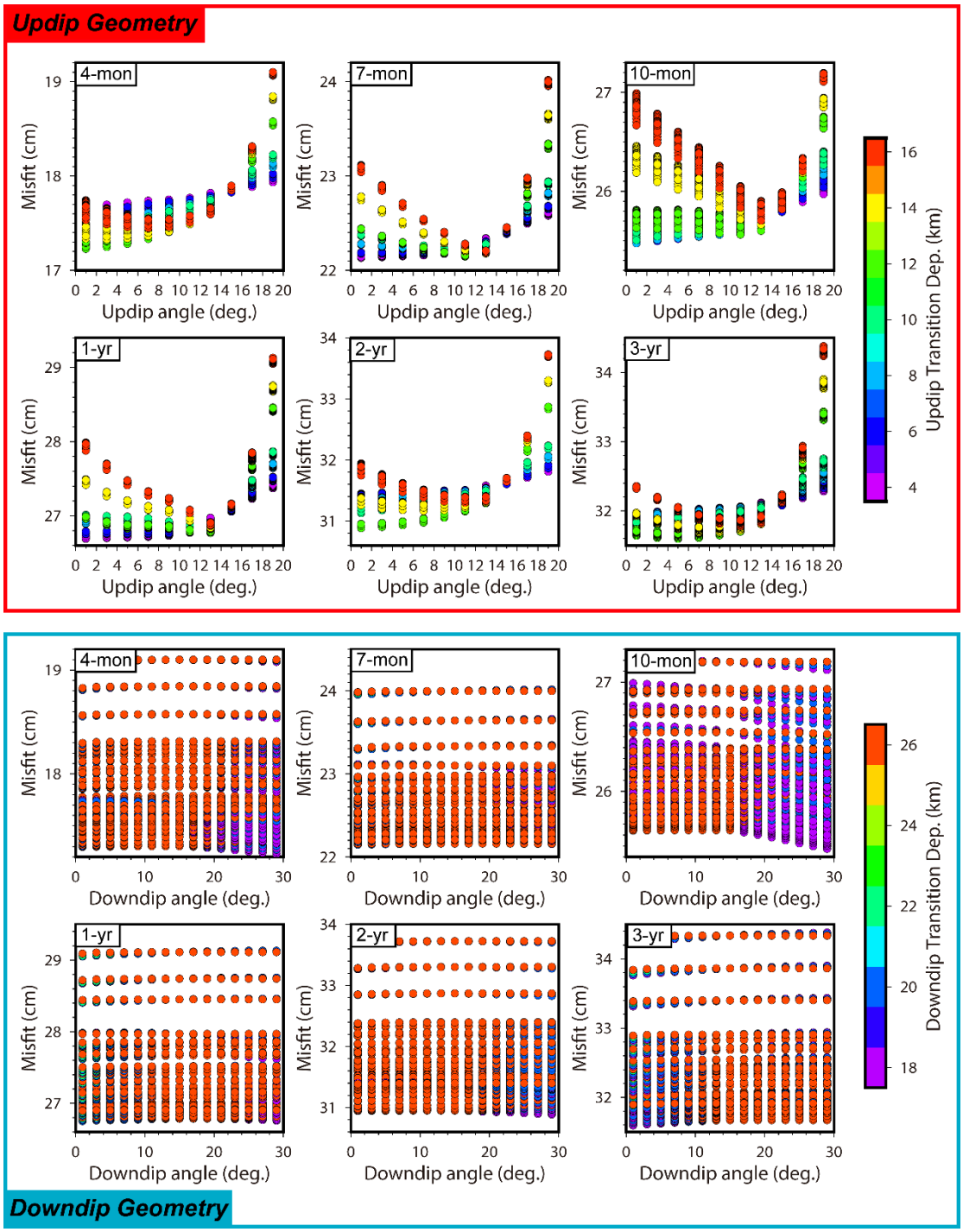

Figure S10. Misfit for searching the dip angles and transition depths of updip and downdip fault geometry with the observations of 4, 7, 10 months and 1, 2, 3 years after the mainshock.

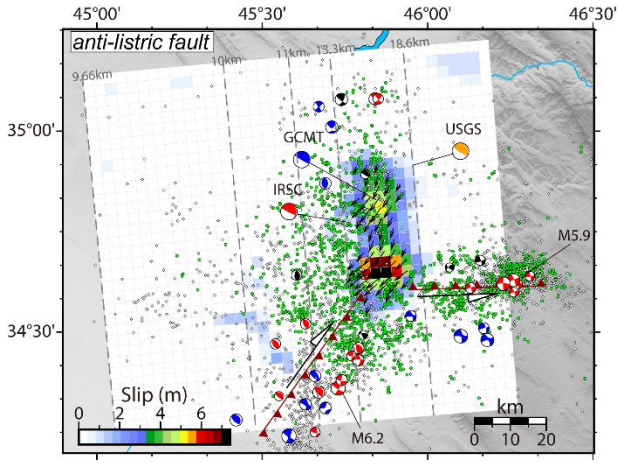

Figure S11. Slip distribution with the anti-listric fault model. The two dark red, strike-slip faults of M 5.9 and M 6.3 events are from Fathian et al. (2021). The green and white dots indicate the relocated aftershocks within about 2 months from Fathian et al. (2021) and aftershocks within about 3 years from Iranian Seismological Center (IRSC, http://irsc.ut.ac.ir). The red, blue and black beach balls are the focal mecha-nisms from IRSC catalogue, Global Centroid Moment Tensor (GCMT) catalogue (https://www.globalcmt.org) and Nissen et al. (2019), respectively.

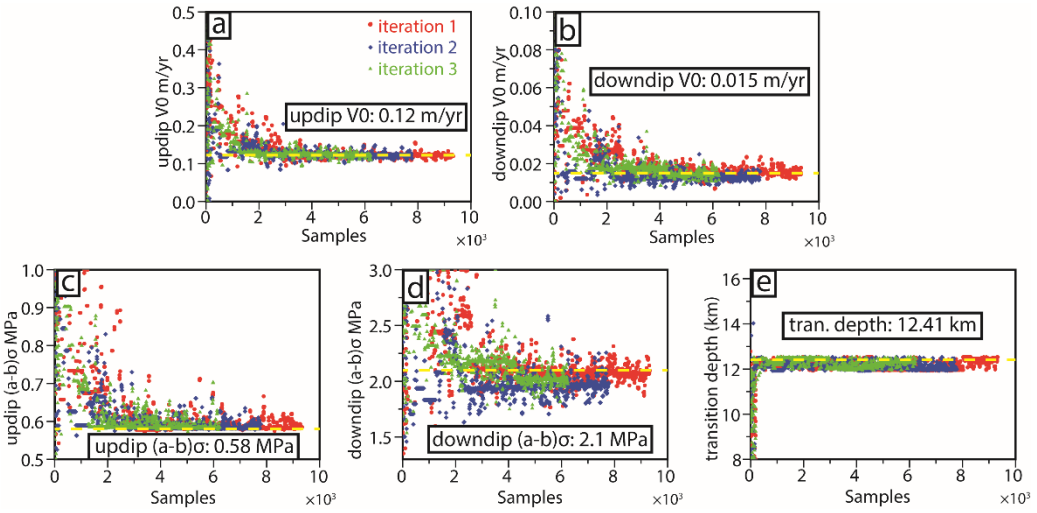

Figure S12. Convergence process with simulated annealing algorithms for updip V_0 and $(a-b)\sigma$ (a and c), downdip V_0 and $(a-b)\sigma$ (b and d) and the transition depth (e), based on the postseismic deformation of 7 months after the mainshock. The yellow dash line represents the optimal parameters.

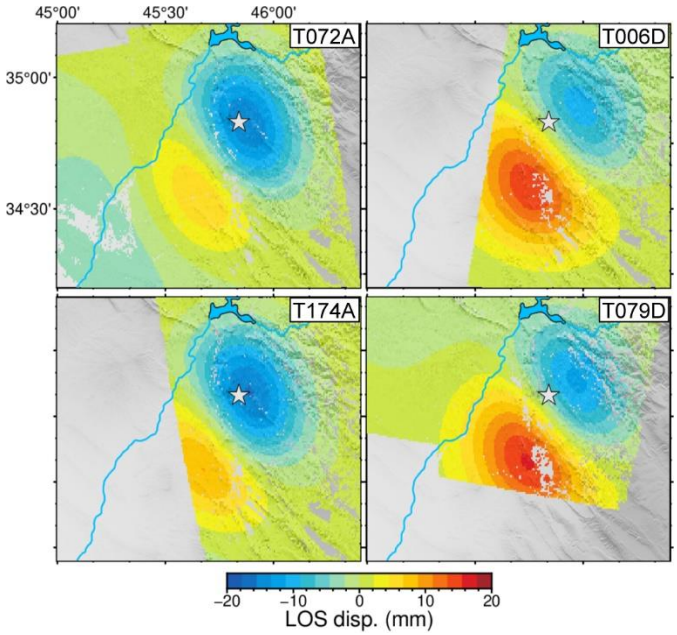

Figure S13. The simulated line-of-sight (LOS) displacements of T072A, T006D, T174A and T079D due to the viscoelastic relaxation 3 year after the mainshock, using a layer model with the best estimates of the rheological viscosity from Lv et al. (2020). The viscoelastic simulations are similar to the results of Wang and Bürgmann (2020). The viscosities of Maxwell lower crust between 30 km to 40 km and Maxwell upper mantle lower than 40 km are 1×10^{19} and 3×10^{19} Pa s, respectively. The gray star is the epicenter of the 2017 Sarpol-e Zahab earthquake.

Table S1. Parameters of Sentinel-1 coseismic interferometric pairs used in this study.

Track	Orbit	Acquisition Time	Perp. Baseline (m)	AZI. Angle (°)	INC. Angle (°)
072	Ascending	Master: 20171111 Slave: 20171117	60.646	-9.909	41.457
006	Descending	Master: 20171107 Slave: 20171119	14.300	189.914	41.419
174	Ascending	Master: 20171106 Slave: 20171118	-1.077	-10.411	36.653
079	Descending	Master: 20171112 Slave: 20171124	46.222	190.408	36.594

Table S2. Data coverage for postseismic time series analysis of each track in this study.

Track	Orbit	Time span		No. of images
		From	To	
072	Ascending	20171123	20201026	83
006	Descending	20171119	20201127	91
174	Ascending	20171118	20201114	90
079	Descending	20171124	20201120	92

Table S3. Nonlinear inversion parameters constraints.

	strike	dip	Depth	width	length	rake
Minimum	340	0	5	5	5	90
Maximum	25	30	25	50	70	180

References

Barnhart, W. D., Brengman, C. M. J., Li, S., & Peterson, K. E. (2018). Ramp-flat basement structures of the Zagros Mountains inferred from co-seismic slip and afterslip of the 2017 Mw7.3 Darbandikhan, Iran/Iraq earthquake. *Earth and Planetary Science Letters, 496*, 96–107. https://doi.org/10.1016/j.epsl.2018.05.036

Fathian, A., Atzori, S., Nazari, H., Reicherter, K., Salvi, S., Svigkas, N., Tatar, M., Tolomei, C., & Yaminifard, F. (2021). Complex co- and postseismic faulting of the 2017–2018 seismic sequence in western Iran revealed by InSAR and seismic data. *Remote Sensing of Environment, 253*. https://doi.org/10.1016/j.rse.2020.112224

Feng, W., Lindsey, E., Barbot, S., Samsonov, S., Dai, K., Li, P., et al. (2017). Source characteristics of the 2015 MW7.8 Gorkha (Nepal)earthquake and its MW7.2 aftershock from space geodesy. *Tectonophysics, 712-713*, 747-758. https://doi.org/10.1016/j.tecto.2016.02.029

Feng, W., Li, Z., Elliott, J. R., Fukushima, Y., Hoey, T., Singleton, A., Cook, R., & Xu, Z. (2013). The 2011 Mw 6.8 Burma earthquake: fault constraints provided by multiple SAR techniques. *Geophysical Journal International, 195*, 650–660. https://doi.org/10.1093/gji/ggt254

Feng, W., Li, Z., Hoey, T., Zhang, Y., Wang, R., Samsonov, S., et al. (2014). Patterns and mechanisms of coseismic and postseismic slips ofthe 2011 Mw7.1 Van (Turkey) earthquake revealed by multi-platform synthetic aperture radar interferometry. *Tectonophysics, 632*,188-198. https://doi.org/10.1016/j.tecto.2014.0 6.011

Feng, W., Samsonov, S., Almeida, R., Yassaghi, A., Li, J., Qiu, Q., Li, P., & Zheng, W. (2018). Geodetic Constraints of the 2017 Mw7.3 Sarpol Zahab, Iran Earthquake, and Its Implications on the Structure and Mechanics of the Northwest Zagros Thrust-Fold Belt. *Geophysical Research Letters, 45*, 6853–6861. https://doi.org/10.1029/2018GL078577

Jónsson, S., Zebker, H., Segall, P., & Amelung, F. (2002). Fault slip distribution of the 1999 Mw7.1 Hector Mine, California, earthquake, estimated from satellite radar and GPS measurements. *Bulletin ofthe Seismological Society of America, 92*(4), 1377–1389. https://doi.org/ 10.1785/0120000922

Lv, X., Amelung, F., Shao, Y., Ye, S., Liu, M., & Xie, C. (2020). Rheology of the Zagros Lithosphere from Post-Seismic Deformation of the 2017 Mw7.3 Kermanshah, Iraq, Earthquake. *Remote Sensing, 12*(2032). https://doi.org/10.3390/rs12122032

Nissen, E., Ghods, A., Karasözen, E., Elliott, J. R., Barnhart, W. D., Bergman, E. A., Hayes, G. P., Jamal-Reyhani, M., Nemati, M., Tan, F., Abdulnaby, W., Benz, H. M., Shahvar, M. P.,

Talebian, M., & Chen, L. (2019). The 12 November 2017 M w 7.3 Ezgeleh-Sarpolzahab (Iran) Earthquake and Active Tectonics of the Lurestan Arc. *Journal of Geophysical Research: Solid Earth, 124*, 2124–2152. https://doi.org/10.1029/2018JB016221

Wang, K., & Bürgmann, R. (2020). Probing fault frictional properties during afterslip updip and downdip of the 2017 Mw 7.3 Sarpol-e Zahab earthquake with space geodesy. *Journal of Geophysical Research: Solid Earth, 125*, e2020JB020319. https://doi.org/ 10.1029/2020JB020319